# Fluidic-Directed Assembly of Aligned Oligopeptides with π-Conjugated Cores

*Amanda B. Marciel, Melikhan Tanyeri, Brian D. Wall, John D. Tovar, Charles M. Schroeder,* and William L. Wilson**

Development of robust strategies for the engineered self-assembly of functional synthetic materials is a major challenge in advanced materials engineering. Biomimetic materials such as synthetic polypeptides and peptide-polymer conjugates serve as model systems that provide insight into the design and engineering of materials with predictable functional properties.[1] Recent advances in synthetic bioorganic chemistry enabled increased control over residue profile, chain length, and functional group placement, thereby facilitating self-assembly of synthetic biopolymers into complex architectures.[2–6] However, the level of complexity of such structures has yet to match those attained by natural polymers (e.g., DNA and peptides) that deterministically self-assemble into functional, three-dimensional hierarchical architectures.[7] As a consequence, directed assembly techniques have emerged as potential new routes towards building supramolecular structures consisting of small molecules, oligomers, and polymers.[8] Prior methods for fluidic-directed assembly using laminar co-flowing streams have shown promise in supramolecular assembly; however, simple laminar co-flows with uniform fluid velocities preclude fine-scale control required for nanostructure alignment. In this work, we report the fluidic-directed assembly of aligned supramolecular structures using planar extensional flow, which induces alignment of underlying material suprastructures due to its dominant extensional/compressional flow character. We demonstrate that microfluidic-based assembly enables reproducible, reliable fabrication of aligned hierarchical constructs that do not form spontaneously in solution. In this way, fluidic-directed assembly of supramolecular structures allows for unprecedented manipulation at the nano- and mesoscale, which has the potential to provide rapid and efficient control of functional materials properties.

In nature, biological polymers form chemically complex and functional heterostructures that underlie life processes. From this perspective, the ability to efficiently harness the assembly of synthetic peptides could offer effective pathways to produce functional materials. To this end, oligopeptide sequences can be appended to synthetic units, such as π-conjugated molecules, thereby adding directionality to their assembly processes. A number of studies have utilized π-conjugated systems in this manner to effectively tune materials properties. For example, organic semiconducting π-conjugated small molecules, oligomers, and polymers are premier candidates for inexpensive semiconductor fabrication due to their readily tunable electronic and optoelectronic properties.[8–11] A variety of template- and solution-based methods including electrospinning and nanolithography have been employed to fabricate π-conjugated organic semiconductors into active devices.[8–11] However, device performance remains hindered in these systems by imprecise morphology. Achieving nano- to mesoscale ordering has become the primary focus of recent efforts,[12–16] wherein π-conjugated structures are constructed by controlling intermolecular orientations via non-covalent π–π, donor/acceptor, and hydrogen bonding interactions, ultimately leading to desired morphology and energy transfer properties. Importantly, these approaches generally lack the absolute control of intermolecular ordering that is imperative for the development of materials with tailored electronic and optoelectronic properties for organic-based devices.[8–11] Here, we report a microfluidic-based strategy for the directed assembly of highly aligned supramolecular structures using planar extensional flows. Assembled synthetic oligopeptide nanostructures are studied using in situ characterization of optical properties during the dynamic assembly process, which offers insight into the assembled hierarchical structures and the assembly kinetics.

We studied the assembly properties of two oligopeptides – DFAA and DFAG – wherein peptide sequences flank π-conjugated oligo(*p*-phenylenevinylene) (OPV) cores (**Figure 1**). In previous work, we developed powerful solid-phase peptide synthesis (SPPS) strategies to incorporate

A. B. Marciel
Center for Biophysics and Computational Biology
University of Illinois at Urbana-Champaign
Urbana, Illinois 61801, USA
Dr. M. Tanyeri
Department of Chemical and Biomolecular Engineering
University of Illinois at Urbana-Champaign
Urbana, Illinois 61801, USA
B. D. Wall, Prof. J. D. Tovar
Department of Chemistry
Johns Hopkins University
Baltimore, Maryland 21218, USA
Prof. C. M. Schroeder
Department of Chemical and Biomolecular Engineering
Center for Biophysics and Computational Biology
Department of Materials Science and Engineering
University of Illinois at Urbana-Champaign
Urbana, Illinois 61801, USA
E-mail: cms@illinois.edu
Prof. W. L. Wilson
Department of Materials Science and Engineering
Frederick Seitz Materials Research Laboratory
University of Illinois at Urbana-Champaign
Urbana, Illinois 61801, USA
E-mail: wlwilson@illinois.edu

**DOI: 10.1002/adma.201302496**

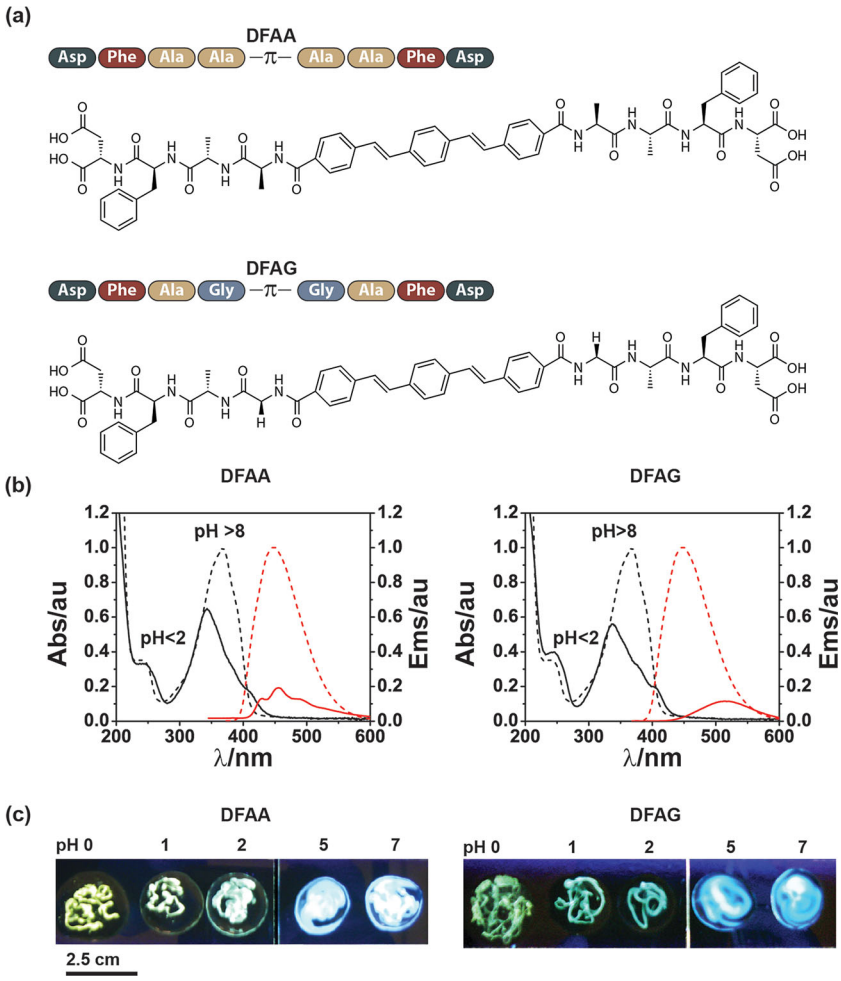


**Figure 1.** Structure and bulk spectral properties of synthetic oligopeptides with π-conjugated cores. a) Schematic and chemical structure of HO-DFAA-OPV-AAFD-OH (DFAA) and HO-DFAG-OPV-GAFD-OH (DFAG). Both oligopeptides contain oligo(*p*-phenylenevinylene) (OPV) cores and are flanked by symmetric amino acid sequences designated by one-letter codes. b) DFAA and DFAG form unaligned networks under acidic conditions resulting in hypsochromic absorption (black) and quenched emission (red), pH > 8 (dashed) and pH < 2 (solid). c) Dispensing DFAA and DFAG through a pipette tip into a pool of HCl at varying concentrations (10–1000 mM) results in one-dimensional macrostructure formation with a bathochromic shift in emission. Macrostructures do not form when dispensed by a pipette into pH 5 (water) or pH 7 buffered solutions.

organic electronic function into self-assembled peptide materials (see Supporting Information).[17] These peptides have the capacity to form amyloid-like fibrils via beta sheet secondary structures and were selected due to their "triggered" supramolecular assembly behavior. OPV provides an ideal conjugated molecular core for assembly studies due to its distinct and well-studied electrical and optical properties when π–π stacking occurs (Figure 1a).[18,19] A limited number of investigations have utilized peptide oligomers with π-conjugated cores for supramolecular assembly.[17,20–24] In general, the electronic properties of these assemblies (e.g., *n*- or *p*-channel activity, fluorescence, excited state transport) are determined by the π-delocalized structures that form through interactions within the molecular core, whereas peptide sequences are chosen to bias their assembly into one-dimensional stacked architectures. The primary forces that drive the assembly of these molecules are the pH-triggered screenings of charged residues that allow for the formation of hydrogen-bonding interactions between the amide carbonyls and protons, and the solvation and π–π interactions of the molecular core components.[17]

DFAA and DFAG (Figure 1a) assemble to form unaligned gel networks under acidic conditions due to protonation of aspartic acid residues, resulting in hypsochromic absorption and quenched bathochromic emission (Figure 1b and Supporting Information). The absorption and emission spectral signatures observed during assembly of DFAA and DFAG are consistent with classic H-aggregate formation.[18,21,25] DFAA gels show a distinct vibronic structure in their fluorescence emission, which arises due to the OPVs twist alignment within the H stack.[19,26] However, DFAG gels show a bathochromic-shifted fluorescence emission, indicative of a charge-transfer emissive state. Interestingly, both DFAA and DFAG gels exhibit qualitatively different properties when these materials are assembled by dispensing through a pipette tip into an acidic solution (10–1000 mM HCl). Upon pipette dispensing, DFAA and DFAG form stable one-dimensional macrostructures. A pH titration (pH 0 to pH 7) of 1 mM DFAA and DFAG shows a bathochromic-shifted emission in acidic conditions, which corresponds to the assembly of one-dimensional macrostructures when processed by pipetting (Figure 1c).

Previous work pioneered by Stupp and co-workers has shown that π-conjugated and amphiphilic peptide oligomers can be aligned by dispensing through a pipette tip, which is known to generate a contraction/expansion flow containing elements of shear and extensional character.[27,28] In this way, pipette processing yields highly aligned macrostructures as observed in SEM images of critical point dried fibers and further evinced by their anisotropic spectral and electrical properties.[27,28] However, it is not possible to consistently and reliably reproduce the 1D macrostructure fabricated by "human-controlled" pipette dispensing. In our work, manually dispensed DFAA and DFAG macrostructures often exhibit random orientations, as evidenced by optical properties identical to those of the unaligned gel networks. From this perspective, there is a strong need for developing controlled microscale processes that can enable efficient and reproducible materials fabrication.

To address the need for controlled processing of functional materials, we developed a microfluidic-based platform to drive the assembly of synthetic oligopeptides (see Supporting Information). Over the last several years, microfluidic systems have been used to achieve exquisite control over patterning and

transport in solution-based processing,[29] with initial demonstrations using laminar flows for assembly of organic polymers, inorganic crystals, and ceramics into one-dimensional structures.[30] Laminar flow provides an ideal environment to assemble materials in a spatially defined manner because fluid streamlines follow deterministic paths in viscous-dominated flows, and interactions between adjacent fluid streams can be controlled by modulating flow rates with straightforward device architectures.[29,31] Recently, microfluidics have been used to create polymer,[32] liquid crystal mesogen,[33] and metal-polymer hybrid 1D structures.[34]

Using a microfluidic device, we assembled DFAA and DFAG into 1D nanostructures using a planar extensional flow generated in a cross-slot geometry.[35,36] We directly observe that planar extensional flow facilitates the consistent formation of one-dimensional synthetic oligopeptide nanostructures at the fluid interface between a pH buffered monomer stream and an acidic stream (**Figure 2**). In the cross-slot device, a flow-focused stream containing synthetic oligopeptide monomer (0.1 mM in buffered solution, pH 7) and an acidic stream (10 mM HCl) are directed into opposing inlet channels and converge at a microchannel junction. Upon initiation of the fluidic-directed assembly process, a bright fluorescent band appears, signifying the formation of a 1D synthetic oligopeptide nanostructure (Figure 2b,c). The dynamics of the assembly process can be followed in real-time using fluorescence microscopy and spectroscopy (see Movie in the Supporting Information). Importantly, we observe that the assembled nanostructure is spectrally distinct from the synthetic oligopeptide monomer, which can be used to monitor the dynamics of nanostructure formation. Using precise hydrodynamic control of the microfluidic platform, we demonstrated the formation of multiple parallel-aligned synthetic oligopeptide nanostructures and their subsequent disassembly (**Figure 3**). In particular, we manipulated the position of the fluid-fluid interface at the microchannel junction by modulating volumetric flow rates in the device; for example, by decreasing the volumetric flow rate of the synthetic oligopeptide stream relative to the flow rate of the acidic stream, we can systematically position the reactive interface across the full range of the cross-slot (Figure 3a). During this process, nanostructures initially formed at the reactive laminar interface are submerged into the advancing acidic stream, thereby preserving the integrity of the preformed nanostructures while initiating formation of an aligned nanostructure at the new interface position (Figure 3a). Distance between synthetic oligopeptide nanostructures is observed to be 38 μm and may be decreased down to 5 μm (Figure 3a).

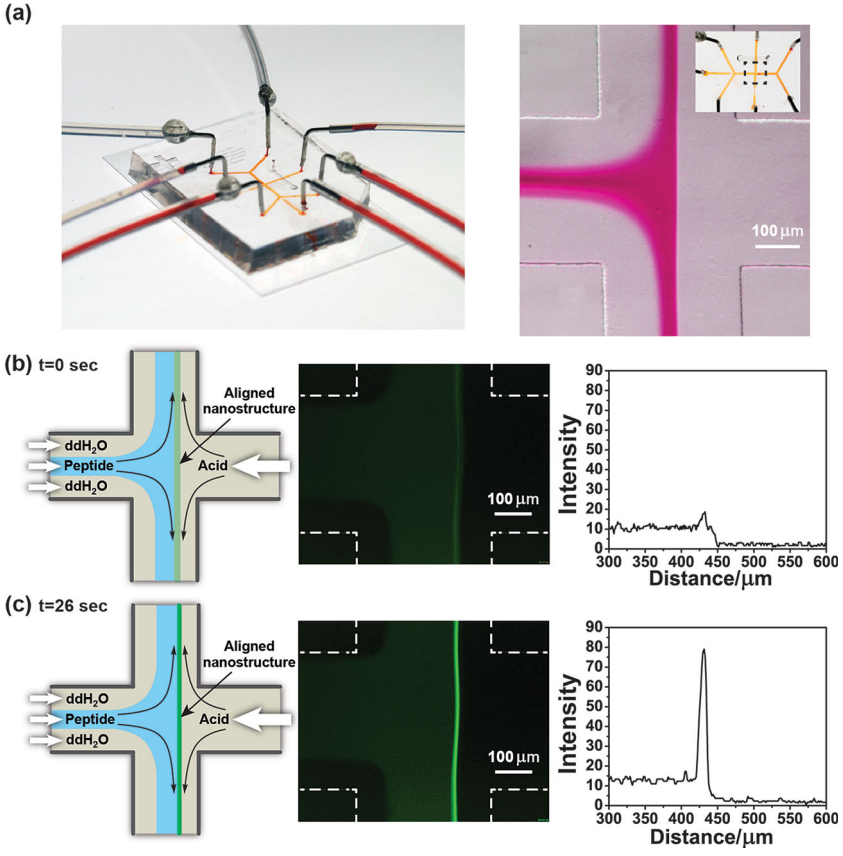


**Figure 2.** Microfluidic platform for synthetic oligopeptide nanostructure formation. a) Photograph and optical micrograph of the experimental microfluidic setup. For display, the channels of the microfluidic device are filled with an orange dye. An optical micrograph of the microchannel junction with red dye flow-focused in water shows experimental conditions used for nanostructure assembly. Inset: overall view of microfluidic device with microchannel junction designated. b) Fluidic-directed assembly of synthetic oligopeptide nanostructures. At time $t$ = 0 s, a 0.1 mM synthetic oligopeptide monomer stream and a 10 mM HCl stream converge at the microchannel junction, thereby forming the initial aligned nanostructure. c) At later times ($t$ = 26 s), a bright fluorescent structure forms, thereby signifying the formation of an aligned nanostructure. Fluorescence intensity analysis using line cut scans show an increase in emission intensity, which denotes nanostructure formation.

In addition to fluidic-directed assembly of single and multiple nanostructures, the microfluidic platform also allows for the disassembly of synthetic oligopeptide nanostructures (Figure 3b). In this experiment, the volumetric flow rate of the synthetic oligopeptide stream was increased relative to the volumetric flow rate of the acidic stream. During this process, the initially formed nanostructure becomes submerged into the neutral synthetic oligopeptide monomer (pH 7), thereby triggering disassembly of the one-dimensional nanostructure (Figure 3b); in this way, a new nanostructure is again formed at the shifted fluid-fluid interface at the microchannel junction. Importantly, we observe that the disassembly process proceeds to completion, as revealed by fluorescence emission intensity analysis of the assembled/disassembled nanostructures (Figure 3b).

Planar extensional flow is an ideal microscale flow to align material structures due to an intrinsic ability to orient and deform macromolecules.[35,36] A planar extensional flow has no rotational character and is

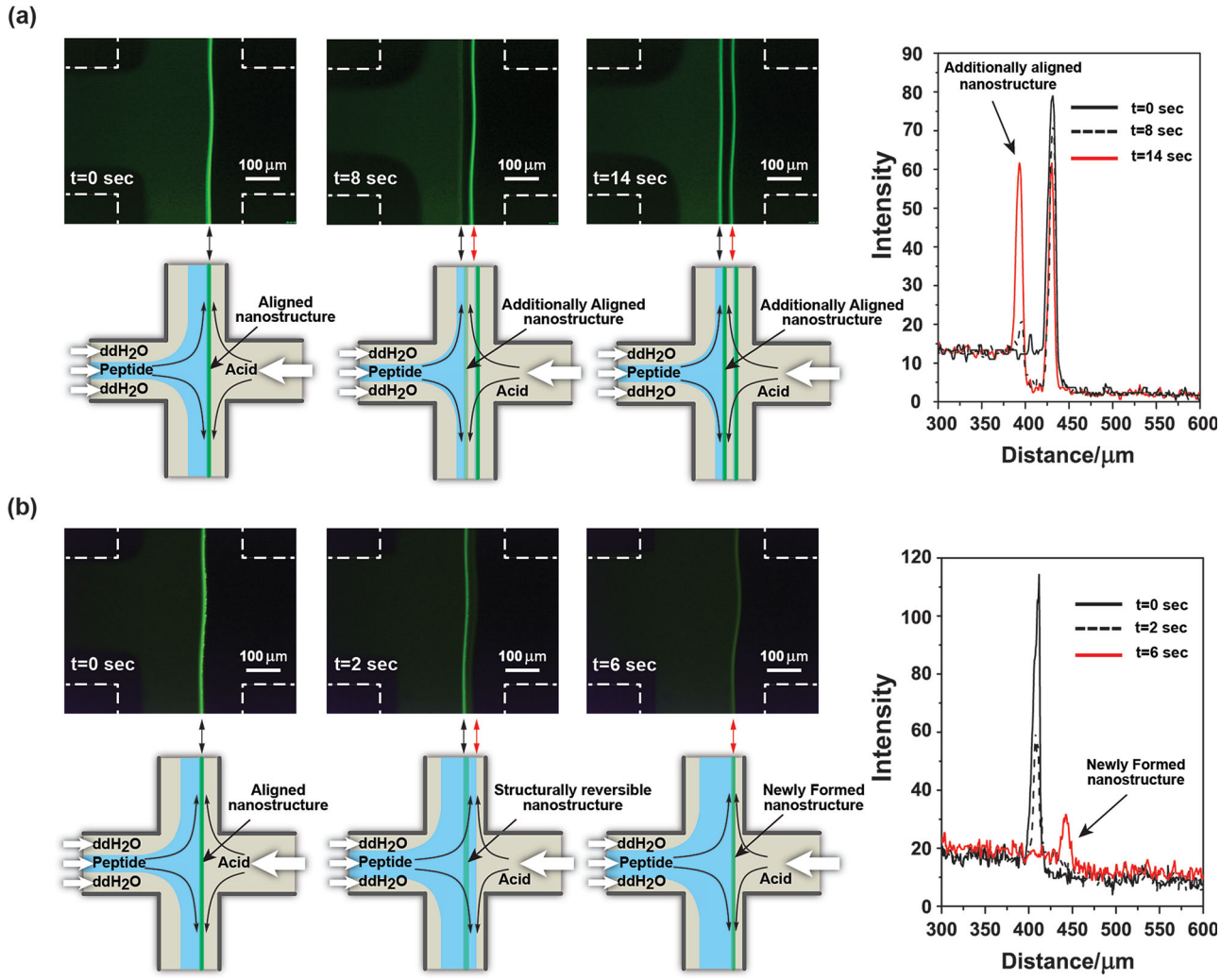


**Figure 3.** Reversible assembly and disassembly of synthetic oligopeptide nanostructures. a) Multiple parallel nanostructures are produced by positioning the fluid-fluid interface via modulating relative volumetric flow rates of the synthetic oligopeptide monomer and acid streams. By decreasing the volumetric flow rate of synthetic oligopeptide monomer relative to the acid stream, additional aligned nanostructures can be produced. Fluorescence intensity line cut scans show the formation of the additional aligned nanostructures. b) Increasing the volumetric flow rate of the synthetic oligopeptide stream relative to the acid stream results in the submersion of the initial nanostructure into pH 7 synthetic oligopeptide monomer solution triggering the disassembly. A new aligned nanostructure is formed at the resulting fluid-fluid interface.

defined by a line of pure fluid extension (outflow axis) and an orthogonal line of pure fluid compression (inflow axis). In this flow field, the fluid velocity varies linearly with position such that $v_x = -Gx$ and $v_y = Gy$, where $G$ is the strain rate and $x$ and $y$ are the distances from the fluid stagnation point along the compressional and extensional axes, respectively.[35] In this way, planar extensional flow is fundamentally different than laminar co-flows where adjacent fluid streams flow in straight channels with approximately uniform velocity profiles near the channel centerline, such that $v_x \approx U \approx$ constant. In both cases, a stable interface is created between two fluid streams in laminar flow conditions (low Reynolds number), wherein viscous forces are significantly greater than inertial forces (see Supporting Information). However, unlike laminar co-flows, planar extensional flow intrinsically provides a velocity gradient along the flow direction that enables simultaneous alignment of microstructure.

Microstructure alignment in planar extensional flow can be understood by comparing relative degrees of diffusion and convection. Polymers and anisotropic suspended Brownian particles are known to orient with fluid flow when convection dominates thermal motion. We can define a rotational Peclet number for the nanostructures $Pe_r \equiv G/D_r$, where the rotational diffusivity is $D_r = 3k_BT(\ln(L/d) - 0.8)/\pi\eta_s L^3$, and $k_BT$ is thermal energy, $\eta_s$ is solution viscosity, and $L$ and $d$ are the nanostructure length and width, respectively. The rotational Peclet number is the ratio of convective forces to thermal forces, and $Pe_r$ of unity denotes the crossover from a diffusion-dominated to a convection-dominated regime.[37] We used steady-state and time-resolved fluorescence microscopy to characterize individual DFAA and DFAG nanostructures assembled at the cross-slot; single nanostructures were found $L = 10$–$100$ μm in length with diffraction-limited widths $d$ (Supporting Information, Figure S4). By treating the assembled synthetic oligopeptide

nanostructures as Brownian rods with length $L$ and diameter $d$, the crossover from diffusion- to convection-dominated behavior occurs for fiber aspect ratios $L/d \approx 10$ with fluid strain rates $G \approx 1$–$30\ s^{-1}$. Therefore, in our experiments, nanostructures are assembled under convection-dominated flow conditions ($Pe_r >> 1$), which suggests that the synthetic oligopeptides comprising the underlying microstructure of assembled materials are highly aligned along the extensional flow (outflow) axis. Planar extensional flows are two-dimensional flows, and microfluidic implementation of such flows typically results in a parabolic flow profile in the $z$-direction, defined as the direction normal to the top and bottom surfaces in the channel, with zero velocity at the boundaries. Due to the high $Pe_r$ conditions, we determined that microstructure alignment occurs infinitesimally close to the surface boundaries (see Supporting Information). Therefore, this microfluidic method allows for near three-dimensional nanostructure alignment and fabrication.

We conducted a series of in situ spectroscopic characterization experiments to verify that the assembled nanostructures formed at the cross-slot are comprised of aligned synthetic oligopeptides (**Figure 4**). Our microfluidic platform allows for real-time monitoring of nanostructure formation using fluorescence microscopy and spectroscopy simultaneously, thereby enabling rapid characterization. Spectra of aligned DFAA nanostructures formed in situ showed pronounced vibronic structure, denoting the formation of an assembled H-type structure consistent with pipette-dispensed gels (Figure 4a). Live spectra of aligned DFAG nanostructures exhibited a quenched bathochromic shift in fluorescence emission (Figure 4b), similar to that observed in static gels. To confirm formation of aligned nanostructures, we utilized fluorescence polarization microscopy (Figure 4c,d). Aligned DFAG nanostructures collected through the outlets of the device show polarization dependent fluorescence emission. An increase in fluorescence signal intensity perpendicular to the nanostructures axis denotes strong orientation of the nanostructure units along the extensional axis, parallel to the outlet channels (Figure 4c). This alignment corresponds to the flow field where birefringence curves align with channel outlets. Moreover this orientation is consistent with the direction of the electronic transition moment expected for the H-aggregate excitons. Previous studies on OPV nanofibers have shown polarization-dependent emission with a peak intensity perpendicular to the nanofiber axis.[38] In addition, aligned nanostructures collected through the outlets of the device display near uniform polarization dependence along the nanostructure (Supporting Information, Figure S5). In a control experiment, we confirmed that polarization dependent emission was not observed for synthetic oligopeptides in neutral or basic solutions processed under the same flow conditions.

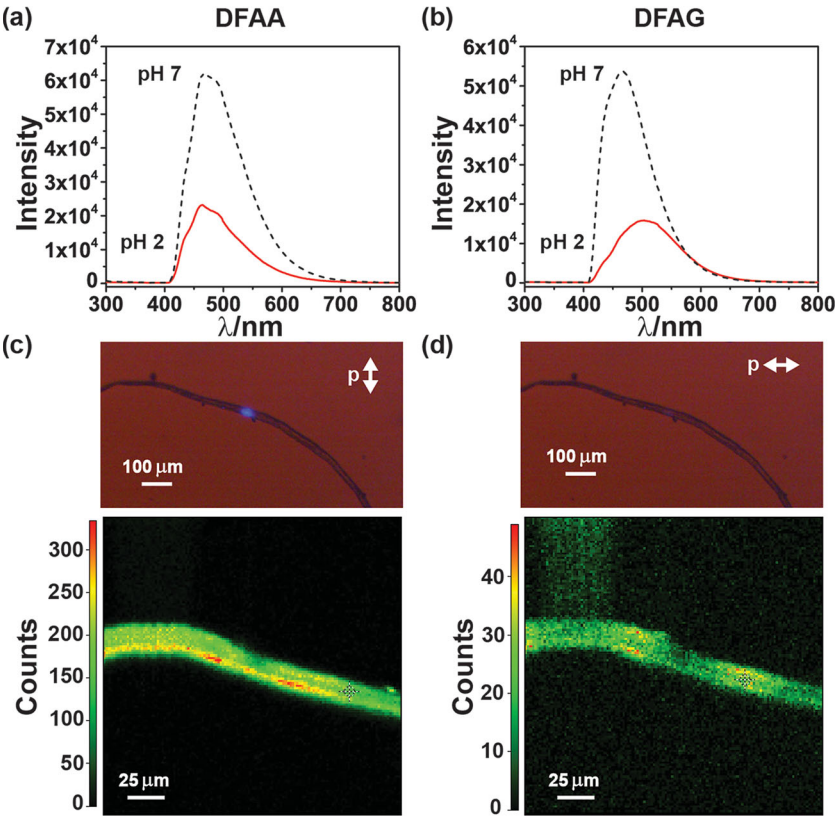


**Figure 4.** In situ spectral characterization of DFAA and DFAG aligned nanostructures. In situ real-time emission spectrum of: a) DFAA and b) DFAG were conducted under basic (pH 7) and acidic (pH 2) conditions. a) At pH 2, DFAA forms aligned nanostructures that result in quenched emission along with the appearance of a vibronic structure (red curve) indicative of the formation of aligned material. b) At pH 2, DFAG aligned nanostructures also result in quenched emission along with a bathochromic shift consistent with the gel and pipette dispensed macrostructures. c,d) Laser excited fluorescence polarization microscopy is used to confirm that nanostructure alignment is correlated to the extensional flow axis (outflow axis). c) DFAG nanostructure shows excitation polarization dependent emission with an increased fluorescence intensity perpendicular to the extensional flow (outflow) axis compared to the fluorescence intensity (d) with excitation polarized parallel to the extensional flow (outflow) axis. The polarization dependence is consistent with aligned nanostructures stacked in an "H aggregate type" geometry.

Fluorescence lifetime imaging microscopy (FLIM) was used to characterize the electronic states of the aligned DFAG nanostructures fabricated in and collected from the microfluidic device (see Supporting Information). Fluorescence lifetimes are highly dependent on the aggregation state of conjugated systems, which ultimately determines the nature of exciton delocalization.[39] Upon photon absorption, conjugated macromolecules may form intrachain (via extended $\pi$-conjugated sections) or interchain (via nearby chains coupling through space) excitons. Disorder in conjugated macromolecules results in exciton trapping, which disrupts delocalization, thereby giving rise to multiexponential decay behavior. We observe that fluorescence lifetimes for aligned DFAG nanostructures can be fit nearly to a single exponential and show a sharp fluorescence lifetime

distribution around 2 ns (Figure S6a,c, Supporting Information). This observation is consistent with a very distinct emissive state, not with a broad distribution of self-trapped states. In previous work, the spectral dynamics of oligopeptides with $\pi$-conjugated cores formed in bulk solution was reported. It was observed that unaligned gels show multiexponential emission decays, with decay time scales ranging from 10–100 ns. The spectral decay dynamics of these unaligned gels are consistent with self-trapped exciton emission observed in amorphous semiconductors and semiconducting polymers. Finally, as control experiments, we performed FLIM measurements of unaligned DFAG gels that show a broad distribution of fluorescence lifetimes consistent with disordered systems (see Supporting Information).

In this work, we demonstrate efficient and reliable aligned supramolecular assembly of synthetic oligopeptides using microscale extensional flows. Simultaneous optical and spectral determination of nanostructure alignment provides a rapid and cost-effective fabrication approach. Alignment of $\pi$-conjugated molecular moieties can give rise to materials properties with desirable electronic transport behavior. Our microfluidic platform allows for the formation and disassembly of multiple, parallel aligned nanostructures, thus facilitating integration of these structures into electronic and optoelectronic devices. Real-time characterization of synthetic oligopeptide assembly kinetics using confocal microscopy along with structural determination via IR-visible sum frequency generation spectroscopy will further our understanding of supramolecular assembly in planar extensional flows. Beyond synthetic oligopeptides, our platform may prove useful to assemble and orient a wide array of small molecules, oligomers, and polymers. In addition, more complex microfluidic architectures may facilitate fabrication of hybrid nanostructures consisting of multiple polymer species, thereby opening up the possibility to tune functional behavior via hydrodynamic forces. In this way, tailored microfluidic technologies are poised to play a key role in controlled assembly of synthetic oligopeptide nanostructures for materials engineering applications.

## Experimental Section

*Microfluidic-Driven Assembly*: The microfluidic devices used for fluidic-directed assembly were hybrid poly(dimethylsiloxane) (PDMS)/glass devices fabricated using standard soft lithography techniques.[40] The design consists of two layers, a control layer and fluidic layer. The fluidic layer has four buffer inlet channels, two outlet channels, and a single sample inlet channel. Inlet buffer channels are split equally on either side of the device, which merge to form two opposing streams at the cross-slot junction. The sample inlet stream is introduced through a separate port and is flow-focused between two adjacent inlet buffer streams, thereby delivering peptide to the center of the microchannel junction. Typical channel dimensions range between 100–500 μm in width and 10–30 μm in height. All the microfluidic experiments were performed at room temperature and consisted of synthetic oligopeptide samples (0.1 mg $mL^{-1}$) in deionized H2O, pH 7. The synthetic oligopeptide samples were introduced via the sample inlet and flow-focused with deionized H2O introduced by the two adjacent buffer inlets. To trigger the pH change and subsequent assembly, HCl (10 mM) was introduced via the remaining two buffer inlets opposing the sample inlet. The microfluidic device was mounted on an inverted microscope (Olympus IX71). Reagents were introduced via two syringe pumps (Harvard Apparatus) with volumetric flow rates in the range of 100–2000 μL $h^{-1}$. The cross-slot of the microfluidic device was imaged using an objective lens (10×, NA = 0.4) and a color CMOS camera (Edmund Optics EO-1312c). The samples were illuminated via a mercury lamp (350/50 nm excitation filter Chroma Technology Corp 31000v2), and resulting fluorescence emission was collected through a 405 nm long pass filter (Semrock BLP01–405R-25) or 578/105 nm single-band band pass filter (BrightLine FF01–578/105–25).

*Fluorescence Emission Spectra Acquisition*: An imaging spectrograph (Princeton Instruments SP2300i with a diffraction grating (1200 lines $mm^{-1}$) and a charge coupled device (CCD) camera (Princeton Instruments PIXIS 1024 7520–0005)) interfaced with an inverted microscope (Olympus IX71) was employed to monitor spectral changes upon assembly at the cross-slot junction. The spectra were acquired at 300–800 nm using an integration time ranging between 10–100 milliseconds.

*Fluorescence Polarization Microscopy*: Initially assembled synthetic oligopeptides were excited with a filtered halogen lamp and imaged at the cross-slot junction using an inverted microscope (Olympus IX71). Emission was collected through a linear polarizer (Thorlabs, LPVISE200-A) aligned parallel and orthogonal to the extensional flow axis of the microfluidic device. To more directly probe the polarization dynamics, polarized laser excitation was also used in a scanning confocal geometry to image polypeptide nanostructures in situ, as well as captured polypeptide. Note: the captured nanomaterial was deposited on a coverslip and sealed with a conventional microscope slide for imaging. An achromatic ½ wave plate in the laser optical path enabled us to rotate the excitation polarization in the specimen plane.

## Supporting Information

Supporting Information is available from the Wiley Online Library or from the author.

## Acknowledgements

The authors acknowledge the use of experimental facilities at the Frederick Seitz Materials Research Laboratory, the Beckman Institute, and the Institute for Genomic Biology at the University of Illinois at Urbana-Champaign. The authors also thank Professor Paul J. A. Kenis for clean-room access for device fabrication. This research was supported by a Packard Fellowship from the David and Lucille Packard Foundation, an NSF carrer award (1254340) to C.M.S. and by the Department of Energy, Office of Basic Energy Sciences (SE-SC0004857) (to J.D.T).

Received: May 31, 2013
Revised: July 18, 2013
Published online: August 21, 2013

[1] M. A. Gauthier, H.-A. Klok, *Chem. Commun.* **2008**, 2591–2611.
[2] C. J. Hawker, K. L. Wooley, *Science.* **2005**, *309*, 1200–1205.
[3] D. J. Hill, M. J. Mio, R. B. Prince, T. S. Hughes, J. S. Moore, *Chem. Rev.* **2001**, *101*, 3893–4011.
[4] G. M. Whitesides, B. Grzybowski, *Science.* **2002**, *295*, 2418–2421.
[5] W. A. Braunecker, K. Matyjaszewski, *Prog. Polym. Sci. (Oxford)* **2007**, *32*, 93–146.
[6] K. T. Nam, S. A. Shelby, P. H. Choi, A. B. Marciel, R. Chen, L. Tan, T. K. Chu, R. A. Mesch, B.-C. Lee, M. D. Connolly, C. Kisielowski, R. N. Zuckermann, *Nat. Mater.* **2010**, *9*, 454–460.
[7] S. Hecht, *Mater. Today* **2005**, *8*, 48–55.
[8] F. J. M. Hoeben, P. Jonkheijm, E. W. Meijer, A. P. H. J. Schenning, *Chem. Rev.* **2005**, *105*, 1491–1546.

[9] A. L. Briseno, S. C. B. Mannsfeld, S. A. Jenekhe, Z. Bao, Y. Xia,, *Mater. Today* **2008**, *11*, 38–47.
[10] F. S. Kim, G. Ren, S. A. Jenekhe, *Chem. Mater.* **2011**, *23*, 682–732.
[11] A. P. H. J. Schenning, E. W. Meijer, *Chem. Commun.* **2005**, 3245–3258.
[12] A. L. Briseno, S. C. B. Mannsfeld, P. J. Shamberger, F. S. Ohuchi, Z. Bao, S. A. Jenekhe, Y. Xia, *Chem. Mater.* **2008**, *20*, 4712–4719.
[13] B. J. Rancatore, C. E. Mauldin, S. -H. Tung, C. Wang, A. Hexemer, J. Strzalka, J. M. J. Fréchet, T. Xu, *ACS Nano* **2010**, *4*, 2721–2729.
[14] Y. Zhang, H. Dong, Q. Tang, S. Ferdous, F. Liu, S. C. B. Mannsfeld, W. Hu, A. L. Briseno, *J. Am. Chem. Soc.* **2010**, *132*, 11580–11584.
[15] L. Pan, G. Yu, D. Zhai, H. R. Lee, W. Zhao, N. Liu, H. Wang, B.C. -K. Tee, Y. Shi, Y. Cui, Z. Bao, *Proc. Natl. Acad. Sci. USA* **2012**, *109*, 9287–9292.
[16] H. Li, B. C. -K. Tee, G. Giri, J. W. Chung, S. Y. Lee, Z. Bao,, *Adv Mater.* **2012**, *24*, 2588–2591.
[17] B. D. Wall, J. D. Tovar, *Pure Appl. Chem.* **2012**, *84*, 1039–1045.
[18] P. Jonkheijm, F. J. M. Hoeben, R. Kleppinger, J. Van Herrikhuyzen, A. P. H. J. Schenning, E. W. Meijer, *J. Am. Chem. Soc.* **2003**, *125*, 15941–15949.
[19] F. J. M. Hoeben, A. P. H. J. Schenning, E. W. Meijer,, *ChemPhysChem.* **2005**, *6*, 2337–2342.
[20] H. Frauenrath, E. Jahnke, *Chemistry* **2008**, *14*, 2942–2955.
[21] R. Matmour, I. De Cat, S. J. George, W. Adriaens, P. Leclère, P. H. H. Bomans, N. A. J. M. Sommerdijk, J. C. Gielen, P. C. M. Christianen, J. T. Heldens, J. C. M. Van Hest, D. W. P. M. Löwik, S. De Feyter, E. W. Meijer, A. P. H. J. Schenning, *J. Am. Chem. Soc.* **2008**, *130*, 14576–14583.
[22] S. R. Diegelmann, J. M. Gorham, J. D. Tovar, *J. Am. Chem. Soc.* **2008**, *130*, 13840–13841.
[23] K. P. R. Nilsson, J. Rydberg, L. Baltzer, O. Inganäs, *Proc. Natl. Acad. Sci. USA* **2003**, *100*, 10170–10174.
[24] J. D. Tovar, *Acc. Chem. Res.* **2013**, in press.
[25] F. C. Spano, *Acc. Chem. Res.* **2010**, *43*, 429–439.
[26] O. Narwark, S. C. J. Meskers, R. Peetz, E. Thorn-Csányi, H. Bässler, *Chem. Phys.* **2003**, *294*, 1–15.
[27] B. D. Wall, S. R. Diegelmann, S. Zhang, T. J. Dawidczyk, W. L. Wilson, H. E. Katz, H. -Q. Mao, J. D. Tovar, *Adv Mater.* **2011**, *23*, 5009–5014.
[28] S. Zhang, M. A. Greenfield, A. Mata, L. C. Palmer, R. Bitton, J. R. Mantei, C. Aparicio, M. O. De La Cruz, S. I. Stupp, *Nat. Mater.* **2010**, *9*, 594–601.
[29] J. Atencia, D. J. Beebe, *Nature* **2005**, *437*, 648–655.
[30] P. J. A. Kenis, R. F. Ismagilov, G. M. Whitesides, *Science* **1999**, *285*, 83–85.
[31] R. F. Ismagilov, A. D. Stroock, P. J. A. Kenis, G. Whitesides, H. A. Stone, *Appl. Phys. Lett.* **2000**, *76*, 2376–2378.
[32] A. L. Thangawng, P. B. Howell Jr, J. J. Richards, J. S. Erickson, F. S. Ligler, *Lab Chip* **2009**, *9*, 3126–3130.
[33] A. R. Shields, C. M. Spillmann, J. Naciri, P. B. Howell, A. L. Thangawng, F. S. Ligler, *Soft Matter* **2012**, *8*, 6656–6660.
[34] J. Puigmartí-Luis, D. Schaffhauser, B. R. Burg, P. S. Dittrich, *Adv Mater.* **2010**, *22*, 2255–2259.
[35] C. M. Schroeder, H. P. Babcock, E. S. G. Shaqfeh, S. Chu, *Science* **2003**, *301*, 1515–1519.
[36] S. J. Haward, M. S. N. Oliveira, M. A. Alves, G. H. McKinley, *Phys. Rev. Lett.* **2012**, *109*, 12.
[37] Ronald G. Larson, *The Structure and Rheology of Complex Fluids*, Oxford University Press, New York **1999**.
[38] C. R. L. P. N. Jeukens, P. Jonkheijm, F. J. P. Wijnen, J. C. Gielen, P. C. M. Christianen, A. P. H. J. Schenning, E. W. Meijer, J. C. Maan, *J. Am. Chem. Soc.* **2005**, *127*, 8280–8281.
[39] G. D. Scholes, G. Rumbles, *Nat. Mater.* **2006**, *5*, 683–696.
[40] M. A. Unger, H.-P. Chou, T. Thorsen, A. Scherer, S. R. Quake, *Science.* **2000**, *288*, 113–116.